Article

Mechanical properties and in-situ deformation imaging of micro-lattices manufactured by laser based powder bed fusion

Anton Du Plessis [1,*], Dean-Paul Kouprianoff [2], Ina Yadroitsava [2] and Igor Yadroitsev [2]

[1] CT Scanner Facility, Stellenbosch University, Stellenbosch, South Africa 7602
[2] Department of Mechanical Engineering, Central University of Technology, Free State, Bloemfontein, South Africa 9300
* Correspondence: anton2@sun.ac.za; Tel.: +27-21-808-9389

Abstract: This paper reports on the production and mechanical properties of Ti6Al4V micro-lattice structures, with strut thickness nearing the single-track width of the laser-based powder bed fusion (LPBF) system used. Besides providing new information on the mechanical properties and manufacturability of such thin-strut lattices, this paper also reports on the in-situ deformation imaging of micro-lattice structures with 6 unit cells in every direction. LPBF lattices are of interest for medical implants, due to the possibility of creating structures with an elastic modulus close to that of the bones and small pore sizes which allow effective osseointegration. In this work four different cubes were produced by laser powder bed fusion and subsequently analyzed using microCT, compression testing and one selected lattice was subjected to in-situ microCT imaging during compression. The in-situ imaging was performed at 4 steps during yielding. The results indicate that mechanical performance (elastic modulus and strength) correlate well with actual density and that this performance is remarkably good, despite the high roughness and irregularity of the struts at this scale. In-situ yielding is visually illustrated.

Keywords: laser powder bed fusion; additive manufacturing; X-ray tomography; in-situ imaging; Ti6Al4V; lattice structures

1. Introduction

Additive manufacturing (AM) is an emerging production technique whereby a part with complex geometry can be produced directly from a design file in a layer-by-layer method [1], [2]. In the case of laser based powder bed fusion (LPBF), a single layer of the part is selectively fused using a laser beam which is scanned across a powder bed surface in a series of tracks, new powder is delivered and the next layer is scanned and fused. Predictably the part integrity requires that single tracks are stable [3] and well overlapped with one another as well as layers to prevent unwanted porosity in solid parts. This has been discussed in some detail in a recent review of the use of X-ray microtomography in additive manufacturing [4]. Despite the possibility of irregularities in parts, it is possible to produce parts with excellent mechanical properties when process parameters are optimized, see for example [5] for biomedical Ti6Al4V produced by LPBF.

One of the major benefits brought about by additive manufacturing is the ability to produce complex parts, and this is especially true for lattice structures which are regularly spaced and repeating combinations of struts with spaces between them. Lattice structures produced by AM have been the topic of many studies in recent years due to the potential to use these in bone replacement implants [6]–[8]. In implants, the porous nature of the lattice structure is beneficial to

 doi:10.20944/preprints201807.0616.v1

lower the elastic modulus of biocompatible materials to match that of the bone at the implant interface, minimizing the possibility for stress shielding causing loss in bone density in the vicinity. Additionally, the open porous nature allows for bone ingrowth into the lattice, effectively ensuring a good bond with the existing bone.

The investigation of the mechanical properties of lattices produced by AM and in particular LPBF is therefore crucial for the adoption of this type of design in implants, along with tailoring its properties for the application of custom shapes which meet local bone density requirements. In general the mechanical properties of these structures can be predicted by the Ashby-Gibson model for open-cell foams [9], [10], with a general relationship for elastic modulus of the lattice (E) as a function of the lattice density (ϱ) and elastic modulus of the solid material used (E_s), given as follows:

$$E = \propto_2 E_s \left(\frac{\rho}{\rho_S}\right)^2$$

Where $\propto_2$ is a value between 0.1 and 4 depending on the lattice geometry [9].

In early work by Parthasarathy et al [11], simple cubic lattices of Ti6Al4V produced by electron beam melting where analyzed by microCT and mechanical testing and it was found that the mechanical properties are weaker than predicted and this was especially so for a model with thinner struts. This might be attributed to manufacturing irregularities such as the rough as-built surface and unexpected porosity inside struts. Geometric accuracy is often a limitation in additive manufacturing of cellular structures, as is the entrapment of powder in the small pores spaces of these structures [1]. Various LPBF cellular structures in Ti6Al4V have been produced in different unit cell designs and their mechanical properties investigated, for example cubic [12], diamond [13], combinations of designs including body-centred cubic [14] and minimal surfaces [15]. Besides variations in mechanical performance induced by geometric inaccuracy and manufacturing errors, slight variations also exist in the properties of various lattice designs themselves. This was demonstrated recently by the numerical analysis of various lattice designs, ignoring manufacturing imperfections [16].

It is therefore clear that the only way to fully understand the complex behavior of lattice structures (with many variations in designs and varying amounts of manufacturing errors, which to some extent also depend on the design), is to use high resolution imaging. In prior work, using relatively large lattices with struts more than 1 mm in diameter, compression tests combined with microCT imaging was used to visualize the first yielding crack locations as shown in [17], with loads up to 140 kN. This was done ex-situ by stopping the mechanical test at first yielding and correlating “before” and “after” microCT scans to find cracks / yielding locations. Some work has also previously been done using in-situ synchrotron tomography during loading of small unit cells produced by LPBF [18]. This work showed local strut-scale deformations during yielding and compared experimental results to those predicted by simulation, but was limited to unit cells which are not necessarily representative of tessellated lattices.

In this work the aim was to investigate the smallest possible lattices that can be produced with a typical LPBF system with track width of roughly 0.1 mm. In addition to investigating the

 doi:10.20944/preprints201807.0616.v1

mechanical properties of such small lattices, the accuracy of these produced micro-lattices may be useful as a reference for future work. Four different sizes of lattice cube samples were produced, each containing 6 unit cells in each direction with a diamond unit cell design with porosity of 80% and unit cell sizes 0.6, 0.8, 1.0 and 1.2 mm. Since the geometry and the density is kept constant, the theoretical elastic modulus and yield stress should be identical in all four cases, therefore the aim was to investigate the properties as the struts become thinner with decreasing unit cell size. The mechanical properties of these small lattices is reported and in-situ imaging of the lattice deformation using high resolution X-ray tomography is demonstrated.

2. Materials and Methods

Models were designed in Materialize Magics and produced from Ti6Al4V using an EOSINT M280 system with standard process parameters for this material. A stress-relief cycle for 3 hours at 650 C [5] was conducted in argon atmosphere after producing the parts, after which the parts were cut from the build plate using electrical discharge machining. The unit cell design used in this work was the diamond design - the unit cell is shown in Figure 1(a). Three samples of each of 4 designs were produced – the computer aided design (CAD) designs are shown in Figure 1(b), with a strut thickness analysis showing that the larger the unit cell, the thicker is the strut as expected. The designs were selected to produce cubes with 6 unit cells in each direction, with unit cell sizes for the 4 designs being 0.6, 0.8, 1.0 and 1.2 mm. This ensures that the density is kept constant and was selected to be 20% dense (80% porosity). The physical sample sizes varied from 3.6 mm to 7.2 mm for the lattice region, and additional solid material was added to the top and bottom to make the total height 8 mm in all cases, for simpler loading in the compression cell.

(a) 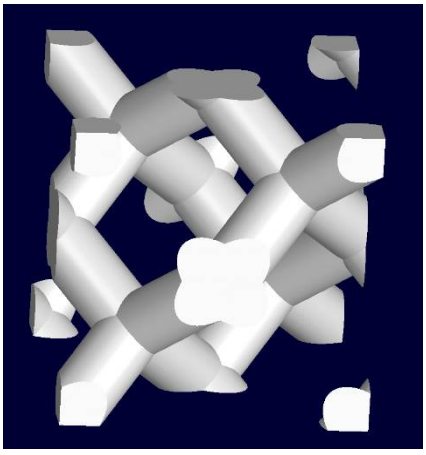

Preprints (www.preprints.org) | NOT PEER-REVIEWED | Posted: 31 July 2018 doi:10.20944/preprints201807.0616.v1

(b)

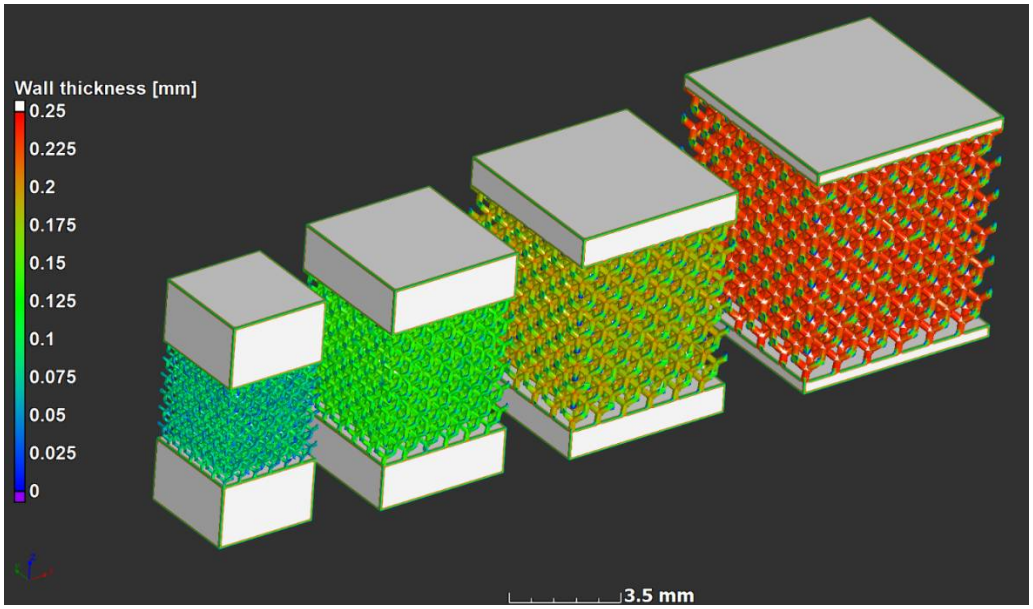

Figure 1: The four CAD designs used – unit cell sizes 0.6, 0.8, 1.0 and 1.2 mm, with strut thickness analysis.

MicroCT scanning was done using laboratory nanoCT as described in [19] using a Deben in-situ loading stage (CT500) in a General Electric Nanotom scanner. The sample sizes in this work were selected according to the maximum sample size of 10 mm and maximum loading force of 500 N of this loading stage. One sample design which did not fail up to 500 N was additionally subjected to compression tests on a different loading stage to obtain the yield strength.

MicroCT voxel size was selected as 4 µm, with 140 kV and 130 µA for X-ray generation, using 0.5 mm copper beam filtration and using continuous scanning mode, a total of 3600 images were recorded during a full rotation of the sample. Images were further analyzed in Volume Graphics VGStudioMax 3.2. Wall thickness analysis used in this work was done with the sphere-method. Due to file sizes and limited computing power, the combined images were resampled in VGStudioMax to 10 µm voxel size and 8 bit data depth to reduce file sizes and memory usage and ease the image analysis.

3. Results and discussion

Samples were manufactured successfully, but microCT analyses show that the strut thickness across the models did not vary as expected – this is shown in Figure 2 using a strut thickness analysis, analogous to Figure 1. Irregularities are expected at this scale due to various practicial limitations which exist when producing small intricate parts during LPBF. The cause of such irregularities can be explained when looking at the minimum size of the designed features with regard to the combined effects of laser spot size, building direction, layer thickness and the implemented scanning strategy for core, overhangs and top surfaces; all having an effect on the amount of detail that can be obtained. Small features are also governed by the single track's width and attached powder particles which in turn are limited by powder particle size distribution. Accuracy of small overhangs is not only dependent on the layer thickness but also on the loose

Preprints (www.preprints.org) | NOT PEER-REVIEWED | Posted: 31 July 2018 doi:10.20944/preprints201807.0616.v1

powder and the inability of the molten pool to penetrate into solid material of the lattice. Therefore irregular surfaces below the struts are expected [20].

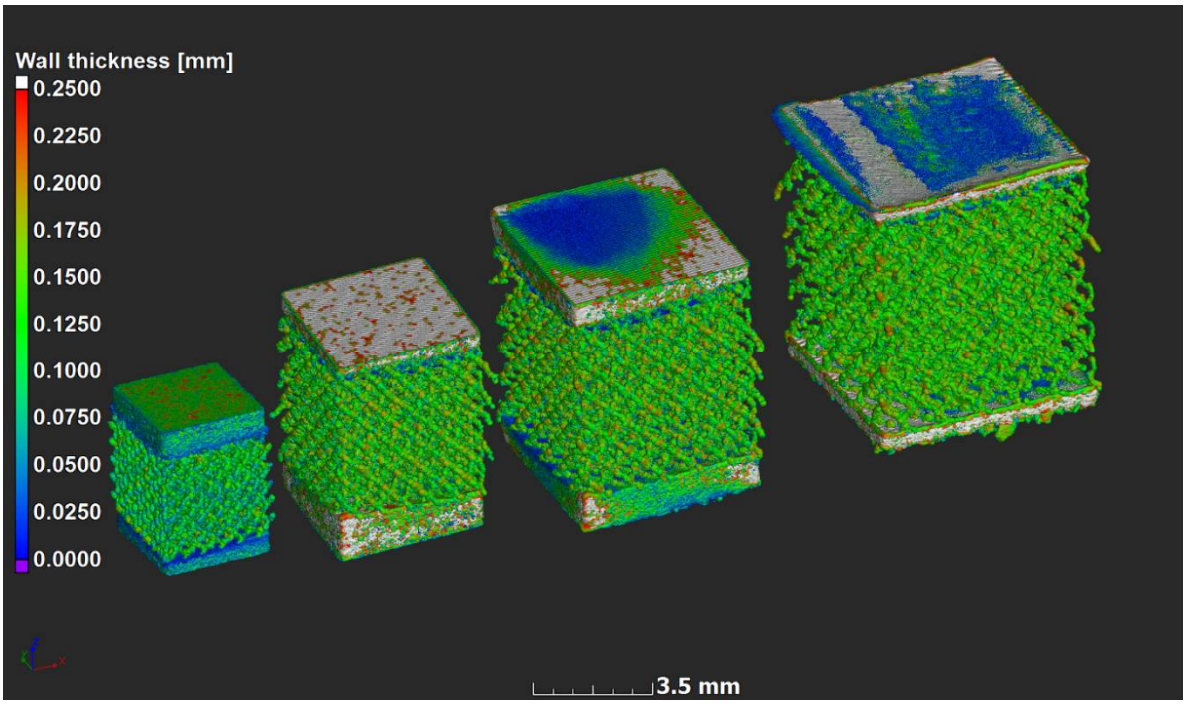

Figure 2: MicroCT scan data 3D rendering with strut thickness colour coding on the micro-lattices. Models with a 0.6, 0.8, 1.0 and 1.2 mm unit cell size from left to right respectively – here the top and bottom of the samples were slightly cropped as the lattice area was scanned only.

The small size of the designed struts, which are close to the single-track width of the laser melting track width, combined with the scanning strategy of the LPBF system used apparently did not allow for variations and these lattices were seemingly all produced with similar strut thickness deviating from the design thickness as shown in Figure 3 (a). The result is that the larger lattice has larger pore spaces making its actual density lower than designed as shown in Figure 3(b).

(a)

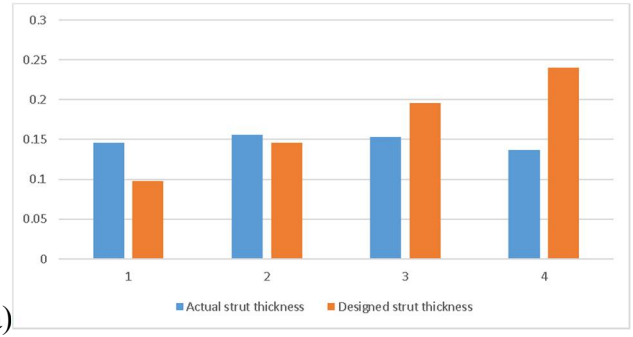

Preprints (www.preprints.org) | NOT PEER-REVIEWED | Posted: 31 July 2018 doi:10.20944/preprints201807.0616.v1

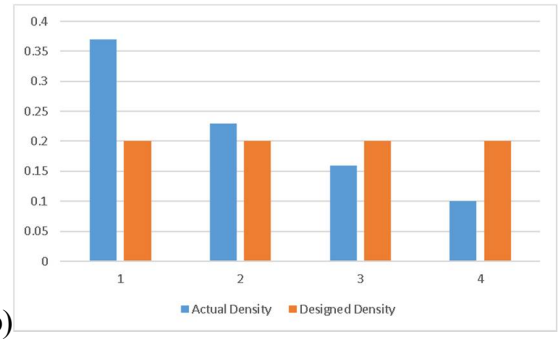

(b)

Figure 3: MicroCT results of actual strut thickness and total density (in blue) compared to the designed values (orange). Strut thickness in mm and density 0-1 on y-axis (fully dense = 1).

As explained in the previous section, the simplified model of Ashby-Gibson for open cell foams indicates a linear correlation between the elastic modulus and the square of the density. This is found experimentally in this case with a slope of approximately 2.5 as shown in Figure 4.

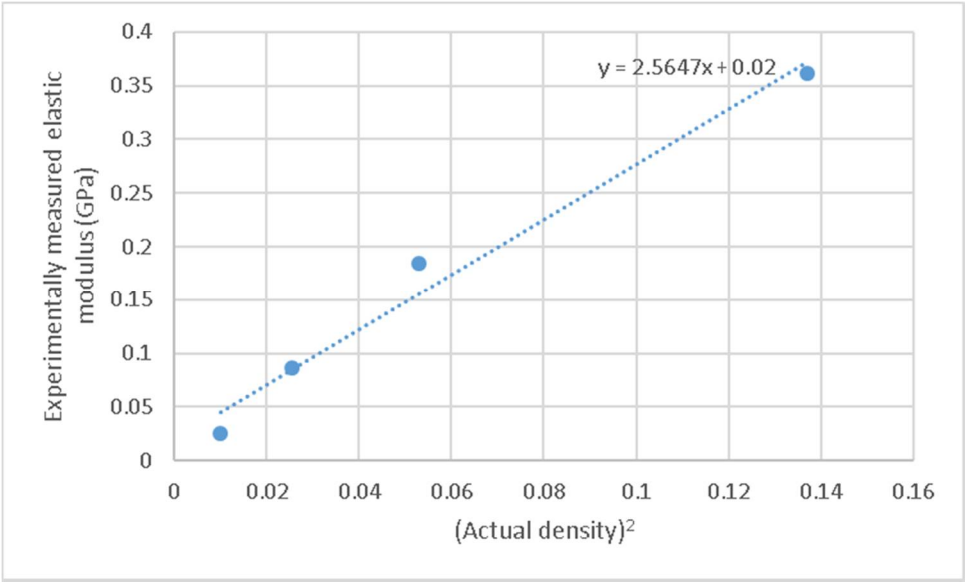

Figure 4: Measured elastic modulus correlates with actual density^2

The value of 2.5 for the slope is within the expected range of 0.1 – 4. Previous work with larger lattices built using the same material process parameters showed that the experimental elastic modulus values were 10 and 20 GPa for 50% density lattice structures of two designs: diagonal and rhombic [17]. This relates to values for alpha (the slope) of 0.35 to 0.7. We can therefore speculate that as the strut thickness reduces, the effect of the rough and irregular surface plays an increasingly important role increasing the slope and making the structure's mechanical properties more sensitive to changes in density. What is interesting to note here is that since the lattice properties follow the density, the smallest lattice of 3.6 mm (unit cell of 0.6 mm) was the strongest – the yield strength is shown in Table 1 together with the actual porosity as measured by microCT. This is due to the similar strut thickness of the 4 models but shorter strut lengths and hence higher density, for the smallest model. This also shows that at this scale the strength and elastic modulus is strongly correlated with the actual porosity (or density).

Preprints (www.preprints.org) | NOT PEER-REVIEWED | Posted: 31 July 2018 doi:10.20944/preprints201807.0616.v1

175

176 **Table 1: Experimental data**

Unit cell design (mm)	Actual porosity (%)	Compressive elastic modulus (MPa)	Compressive strength (MPa)	Maximum load (N)
0.6	63	361	53	688
0.8	77	185	9.5	220
1.0	84	87	7.6	110
1.2	90	25	1.0	50

177

178 In-situ compression allowed imaging of the same lattice prior to full densification – first before
179 loading, then directly after initial yielding, and at a few more representative steps during yielding.
180 This is shown in Figure 5, where red arrows indicate the positions where the loading was stopped
181 and microCT scans were performed. The resulting microCT data is represented for the aligned
182 volumes, with side-by-side slice images through the middle of the lattice, and with 3D views of the
183 entire lattice. These images indicate that yielding occurs gradually and progressively as struts
184 collapse in this type of lattice.

185

186 (a)

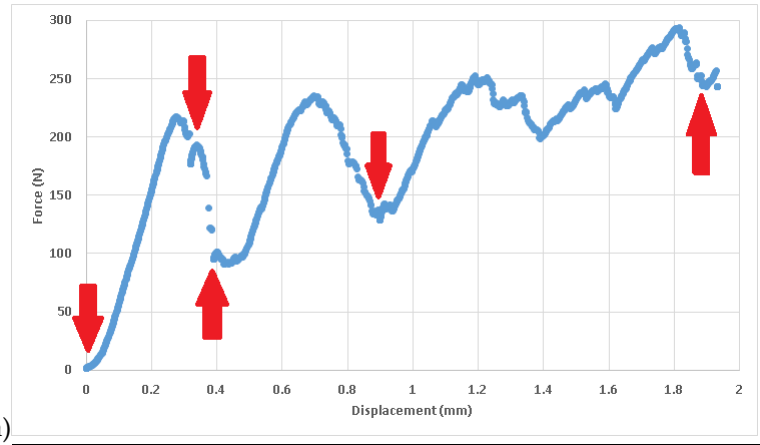

187 (b)

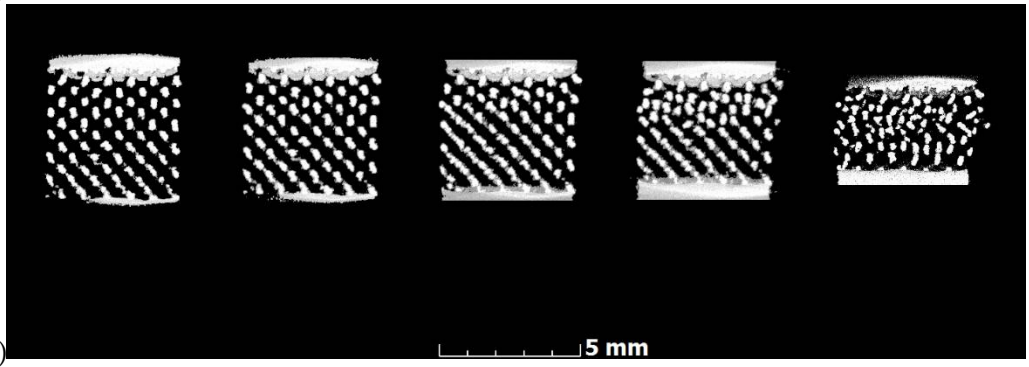

Preprints (www.preprints.org) | NOT PEER-REVIEWED | Posted: 31 July 2018 doi:10.20944/preprints201807.0616.v1

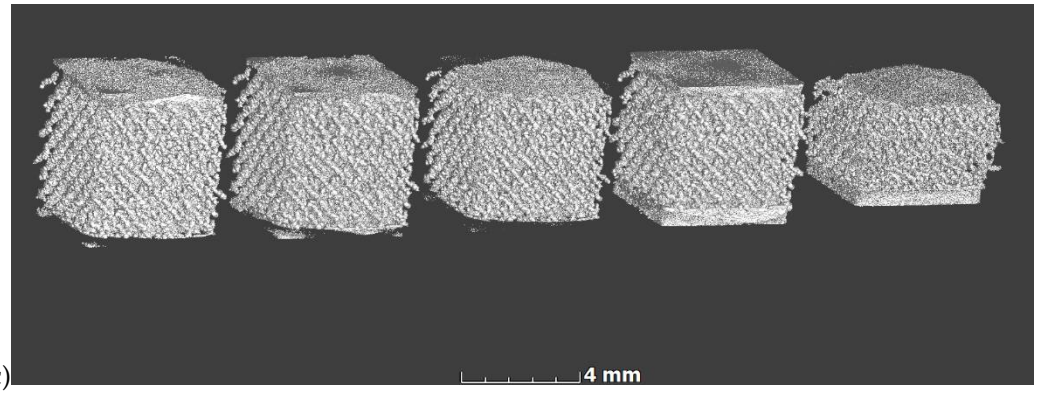

(c)

Figure 5: In situ deformation imaging of a lattice (0.8 mm unit cell) at the selected points during yielding – steps according to arrows in force-displacement curve.

The alignment of the scans is simplified by the fact that the sample stays in the same location in the scan system, and as the load cell works by moving the bottom upwards, the deformation can be imaged more closely on individual struts by making the unloaded scan transparent and visualizing the loaded image. This is done in Figure 6 for a small section (approx. 0.5 mm) to visualize the deformation and collapse of individual struts, in this case taken from the middle near the top of the sample, where collapse first occurred. The light blue transparent struts shown in Figure 6 show the unloaded sample while the third scan in the series is shown here in solid rendering (this is at the first yield dip – the third arrow in Figure 5). The colour coding applied to the loaded sample image is a nominal-actual comparison - this quantitatively shows the deformation value (in red is where largest deformation is relative to the unloaded sample). Besides collapse, the largest deformations occur at the strut junctions. The three images are the same region from different viewing angles.

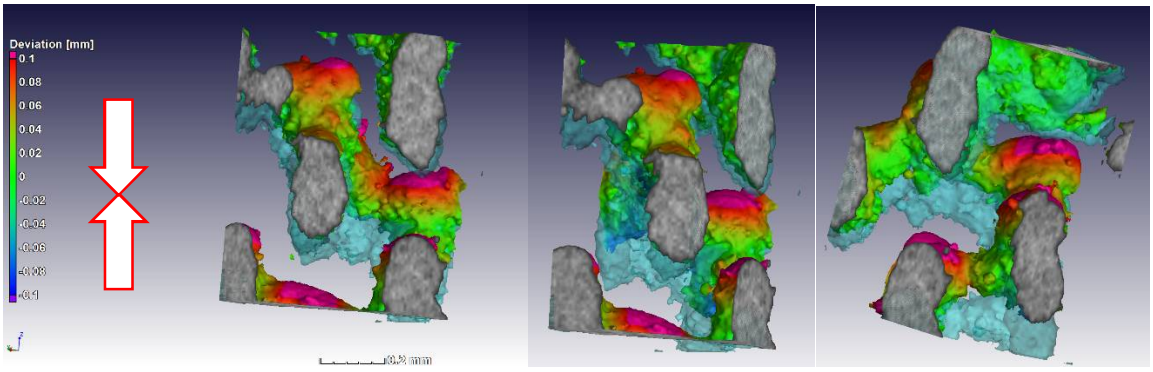

Figure 6: Three different angular views of the same internal location showing yielding behavior of individual struts and colour coding indicating largest deformation relative to unloaded state (deformation upwards in image, unloaded state semi-transparent blue). Loading direction indicated by arrows.

5. Conclusions

This paper reported the mechanical properties of a series of micro-lattices with struts near the single track width of the laser powder bed fusion system used to produce them. The results show that such lattices can be produced successfully but the small strut thickness deviates from the designed

value. It was shown that the mechanical properties of micro lattices produced by LBPF are strongly dependent on actual density irrespective of strut thickness and length; and can therefore be predicted with some confidence using this measure alone. Compared to larger lattices, the dependence of the mechanical properties is stronger with density (higher slope in the Ashby-Gibson equation). In-situ microCT imaging demonstrated strut collapse and yielding occurring in the middle of the tessellated lattice structure first. These images represent the first in-situ images of a full micro-lattice structure's yielding behavior. The method will be useful to investigate and compare the complex yielding behavior of different lattice designs and materials.

Author Contributions: Conceptualization, AdP; Methodology, AdP, IY1,IY2; Software, AdP; Validation, AdP,DK; Formal Analysis, All; Investigation, AdP; Resources, All; Data Curation, All; Writing-Original Draft Preparation, AdP; Writing-Review & Editing, All; Visualization, All.

Funding: This research received no external funding.

Conflicts of Interest: The authors declare no conflict of interest.

References

1. M. Schmidt et al., "Laser based additive manufacturing in industry and academia," CIRP Ann., vol. 66, no. 2, pp. 561–583, Jan. 2017.
2. T. Debroy et al., "Additive manufacturing of metallic components – Process, structure and properties," 2017.
3. I. Yadroitsev, A. Gusarov, I. Yadroitsava, and I. Smurov, "Single track formation in selective laser melting of metal powders," J. Mater. Process. Technol., vol. 210, no. 12, pp. 1624–1631, Sep. 2010.
4. A. du Plessis, I. Yadroitsev, I. Yadroitsava, and S. le Roux, "X-ray micro computed tomography in additive manufacturing: a review of the current technology and applications," 3D Print. Addit. Manuf., vol. In press, 2018.
5. I. Yadroitsev, P. Krakhmalev, I. Yadroitsava, and A. du Plessis, "Qualification of Ti6Al4V ELI Alloy Produced by Laser Powder Bed Fusion for Biomedical Applications," JOM, 2018.
6. X. P. Tan, Y. J. Tan, C. S. L. Chow, S. B. Tor, and W. Y. Yeong, "Metallic powder-bed based 3D printing of cellular scaffolds for orthopaedic implants: A state-of-the-art review on manufacturing, topological design, mechanical properties and biocompatibility," Mater. Sci. Eng. C, vol. 76, pp. 1328–1343, Jul. 2017.
7. X.-Y. Zhang, G. Fang, and J. Zhou, "Additively Manufactured Scaffolds for Bone Tissue Engineering and the Prediction of their Mechanical Behavior: A Review," Materials (Basel)., vol. 10, no. 1, p. 50, Jan. 2017.
8. G. Dong, Y. Tang, and Y. F. Zhao, "A Survey of Modeling of Lattice Structures Fabricated by Additive Manufacturing," J. Mech. Des., vol. 139, no. 10, p. 100906, Aug. 2017.
9. L. Gibson and M. Ashby, "Cellular solids: structure and properties," 1999.
10. M. Ashby, T. Evans, N. Fleck, and J. Hutchinson, Metal foams: a design guide. 2000.
11. J. Parthasarathy, B. Starly, S. Raman, and A. Christensen, "Mechanical evaluation of porous titanium (Ti6Al4V) structures with electron beam melting (EBM)," J. Mech. Behav. Biomed. Mater., vol. 3, no. 3, pp. 249–259, Apr. 2010.
12. E. Sallica-Leva, A. L. Jardini, and J. B. Fogagnolo, "Microstructure and mechanical behavior of porous Ti–6Al–4V parts obtained by selective laser melting," J. Mech. Behav. Biomed. Mater., vol. 26, pp. 98–108, Oct. 2013.
13. S. M. Ahmadi et al., "Mechanical behavior of regular open-cell porous biomaterials made of diamond lattice unit cells," J. Mech. Behav. Biomed. Mater., vol. 34, pp. 106–115, Jun. 2014.
14. S. Ahmadi et al., "Additively Manufactured Open-Cell Porous Biomaterials Made from Six Different Space-Filling Unit Cells: The Mechanical and Morphological Properties," Materials (Basel)., vol. 8, no. 4, pp. 1871–1896, Apr. 2015.
15. F. S. L. Bobbert et al., "Additively manufactured metallic porous biomaterials based on minimal surfaces: A unique combination of topological, mechanical, and mass transport properties," Acta Biomater., vol. 53, pp. 572–584, Apr. 2017.
16. A. du Plessis, I. Yadroitsava, I. Yadroitsev, S. le Roux, and D. Blaine, "Numerical comparison of lattice unit cell designs for medical implants by additive manufacturing," Virtual Phys. Prototyp., pp. 1–16, Jun. 2018.

17. A. du Plessis, I. Yadroitsava, and I. Yadroitsev, "Ti6Al4V lightweight lattice structures manufactured by laser powder bed fusion for load-bearing applications," Opt. Laser Technol., vol. In press, 2018.
18. H. D. Carlton et al., "Mapping local deformation behavior in single cell metal lattice structures," Acta Mater., vol. 129, pp. 239–250, May 2017.
19. A. du Plessis, S. G. le Roux, and A. Guelpa, "The CT Scanner Facility at Stellenbosch University: An open access X-ray computed tomography laboratory," Nucl. Instruments Methods Phys. Res. Sect. B Beam Interact. with Mater. Atoms, vol. 384, 2016.
20. D. Kouprianoff, A. du Plessis, I. Yadroitsava, I. Yadroitsev. Destructive and nondestructive testing on small and intricate SLM components. In Proc. RAPDASA 18th International Conference, Durban, Inkosi Albert Luthuli International Convention Centre, November 8- 10, 2017